Thrusters Pairing Guidelines for Trajectory Corrections of Projectiles

Daniel Corriveau*
Canadian Department of National Defence, Quebec City, Quebec G3J 1X5, Canada
and
Pierre Wey† and Claude Berner†
ISL, French–German Research Institute of Saint-Louis, 68301 Saint-Louis, France

DOI: 10.2514/1.51811

A novel method for correcting the trajectory of spin- and fin-stabilized projectiles using pairs of impulse thrusters located away from the center of mass is described in this paper. The impulses are generated from the detonation of a very small quantity of explosive. By locating the impulse thrusters away from the center of mass, it is possible to significantly increase the trajectory correction. This is explained by the fact that, in such a case, the deflection results from the aerodynamic jump due to the projectile oscillation in addition to that of the impulses. An optimal combination of thrusters can be achieved by considering pairs of impulses that have the double objective of maximizing the deflection and minimizing the drag due to the oscillations. In this paper, the linear theory of ballistics is used to develop an analytical model representing the motion of a projectile subjected to impulse thrusters. Using the linearized equations of angular motion and considering ideal cases, the optimization scheme for using double impulses is defined by a set of three rules. The latter are then assessed in the case of actual projectiles, using six-degree-of-freedom computations. The course correction process for a 30-mm fin-stabilized air-defense projectile and a standard 105-mm spin-stabilized artillery shell are presented.

Nomenclature

A	=	projectile reference area; $\pi d^2/4$, m^2
a	=	angular deflection of trajectory, rad
C_D	=	drag coefficient
C_{D2}	=	square-yaw drag coefficient
$C_{L\alpha}$	=	lift force coefficient
$C_{Mp\alpha}$	=	Magnus moment coefficient
C_{Mq}	=	pitching damping moment coefficient
$C_{M\alpha}$	=	pitching moment coefficient
$C_{Np\alpha}$	=	Magnus force coefficient
d	=	projectile reference caliber, m
I_x	=	projectile axial moment of inertia, kg · m^2
I_y	=	projectile transverse moment of inertia, kg · m^2
J	=	impulse vector due to thruster, N · s
J_{D_2}	=	impulse vector due to quadratic-yaw drag force, N · s
J_L	=	impulse vector due to lift force, N · s
J_Y	=	impulse vector due to Magnus force, N · s
K_{S0}, K_{F0}	=	initial amplitude of slow and fast epicyclic yaw arm, rad
l_{CJ}	=	distance from center of mass to location of applied impulse, cal (positive toward nose, negative toward boattail)
m	=	projectile mass, kg
p	=	projectile axial spin, s^{-1}
s	=	distance traveled along flight path, cal
V	=	projectile velocity, m · s^{-1}
α	=	pitch angle, rad
$\bar{\alpha}$	=	total incidence angle, rad
β	=	yaw angle, rad
λ_S, λ_F	=	slow and fast arm damping rate, cal^{-1}
ξ	=	complex incidence
ξ_0	=	initial yaw, rad
ξ_0'	=	initial yaw rate, rad/cal
ρ	=	air density, kg/m^3
ϕ	=	orientation of vectors defined in pitch-yaw plane, rad
ϕ_S', ϕ_F'	=	slow and fast arm turning rate, rad/cal

I. Introduction

THIS work had for an objective the development of a better understanding of the use of impulsers on fin- and spin-stabilized projectiles and their impact on the aerodynamics of these ammunitions. The Guided Supersonic Projectile (GSP) project is focused on the guidance and control of a medium-caliber fin-stabilized shell designed for short-range air-defense engagements (see [1–3]). The Artillery Precision Guided Munition project investigates the guidance of conventional spin-stabilized 105-mm artillery shells. The impulse thrusters consist of small detonators that generate a high force for a very short period of time. The impulse thrusters differ significantly from the more conventional jet thrusters, in that the impulse is created by the detonation of explosive material as opposed to accelerating a gas through a nozzle. The impulsers or impulse thrusters are being developed and manufactured in house. The thrusters will be mounted inside the projectile at a specific axial location in a ringlike fashion. They will be used to divert the projectile laterally.

Considering the use of Dirac lateral impulses as a promising technique to control both fin- and spin-stabilized shells, Wey and Corriveau have developed an analytical model as a first approach to assess the performance of the course correction [4].

Research and development on the use of thrusters or reaction jets to improve the precision of fin-stabilized projectiles, such as missiles and rockets, has been going on for decades. Over the years, a significant amount of research was performed to understand the interaction of the reaction jets with the projectile external flow, as demonstrated by Champigny and Lacau [5]. Furthermore, several investigators studied the loads caused by lateral pulse jets on a

Received 29 July 2010; revision received 12 January 2011; accepted for publication 12 January 2011.

*Defence Scientist, Defence Research and Development Canada–Valcartier, Precision Weapons Section, 2459 Pie-XI Boulevard North. Member AIAA.

†Research Scientist, Exterior Ballistics Group, P.O. Box 70034.

Report Documentation Page

Form Approved
OMB No. 0704-0188

1. REPORT DATE	2. REPORT TYPE	3. DATES COVERED
2011		**00-00-2011 to 00-00-2011**

4. TITLE AND SUBTITLE	5a. CONTRACT NUMBER
Thrusters Pairing Guidelines for Trajectory Corrections of Projectiles	5b. GRANT NUMBER
	5c. PROGRAM ELEMENT NUMBER
6. AUTHOR(S)	5d. PROJECT NUMBER
	5e. TASK NUMBER
	5f. WORK UNIT NUMBER
7. PERFORMING ORGANIZATION NAME(S) AND ADDRESS(ES) **Canadian Department of National Defence,Precision Weapons Section,2459 Pie-XI Boulevard North,Quebec City, Quebec G3J 1X5, Canada,**	8. PERFORMING ORGANIZATION REPORT NUMBER
9. SPONSORING/MONITORING AGENCY NAME(S) AND ADDRESS(ES)	10. SPONSOR/MONITOR'S ACRONYM(S)
	11. SPONSOR/MONITOR'S REPORT NUMBER(S)

12. DISTRIBUTION/AVAILABILITY STATEMENT
Approved for public release; distribution unlimited

13. SUPPLEMENTARY NOTES

14. ABSTRACT

15. SUBJECT TERMS

16. SECURITY CLASSIFICATION OF:			17. LIMITATION OF ABSTRACT	18. NUMBER OF PAGES	19a. NAME OF RESPONSIBLE PERSON
a. REPORT **unclassified**	b. ABSTRACT **unclassified**	c. THIS PAGE **unclassified**	**Same as Report (SAR)**	**9**	

projectile body. Brandeis and Gill [6] performed an experimental study on the effect of a lateral jet on the forces and moments on a supersonic missile.

For spin-stabilized projectiles, the use of impulsers is not as common, so the technology is still very much in the development phase. Horwath and Barnych [7] presented a concept of a low-cost course correction (LCCC) technique applied to a 40-mm projectile that makes use of impulsers. Magnotti et al. [8] tested similar LCCC fuses on an experimental mortar projectile. Flight-path corrections of up to 6.0 mils were obtained using an impulse of 2.6 Ns.

Research on the impact of thrusters or impulsers on the flight dynamics of spinning projectiles is very scarce in the open literature. Using the projectile linear theory, Cooper [9] has analytically shown that the effect of an impulse on a spinning projectile produced an additive contribution to the usual aerodynamic jump of the free-flight projectile with no applied impulse. Burchett et al. [10] developed closed-form expressions for the swerving motion of a dual-spin projectile in atmospheric flight under the action of lateral pulse jets. For nonrolling projectiles, Guidos and Cooper [11] extended the existing analytical theory for quantifying the free-flight motion to include the effect of a simple lateral impulse applied during flight. Ollerenshaw and Costello [12] explained in detail the swerve response of fin- and spin-stabilized projectiles subjected to a control force. A good understanding of such swerve response is fundamental to implementing the pairing technique presented in the current paper.

Research and development are currently ongoing in order to increase the magnitude of the impulse generated by thrusters and to reduce the size of these devices. An example of such work is that of English et al. [13], who developed a high-power short-duration microelectromechanical-systems-sized gas generator actuator for spinning projectiles.

The objective of this study consisted of developing a control scheme for the control of projectiles using pairs of impulse thrusters. In the first part of the paper, the concept of impulse pairing to achieve effective control of a spin- and fin-stabilized projectile is introduced. The theoretical background of the pairing method is explained in the case of ideal projectiles. Three basic rules are presented to ensure successful pairing of impulse thrusters to maximize lateral corrections.

The second part of the paper presents the results from six-degree-of-freedom (6-DOF) computations applied to the actual parameters of a generic 105-mm artillery shell and a medium-caliber air-defense projectile, which is called the 30-mm fin-stabilized GSP shell. Compared with the analytical results presented in Wey and Corriveau [4], 6-DOF computations take into account the variations in the projectile velocity and aerodynamic coefficients during the flight. These simulations serve to validate the use of the impulse pairing process as a viable projectile control alternative.

II. Analytical Model

Using the linear theory of ballistics, an analytical model was developed in order to predict the projectile angular motion and velocity resulting from the activation of thrusters. In developing the model, the following hypotheses were made: the total incidence of the projectile is small (i.e., $\tan\bar{\alpha} < 0.1$), the magnitude of the projectile velocity is constant, and the aerodynamic coefficients and the inertial parameters of the projectile are constant.

A. Angular Motion Equation

Neglecting the steady-state yaw due to gravity, introducing the effect of the impulse and shifting the origin of the flight path to the impulse location ($s = 0$), the epicyclic pitching and yawing motion of a projectile can be represented by the following differential equation (McCoy [14]):

$$\xi'' + (H - iP)\xi' - (M + iPT)\xi = \xi_0'\delta(s) \tag{1}$$

where $\xi = \alpha + i\beta$ is the complex incidence, and the superscript prime denotes differentiation with respect to the flight path s. The variable $\delta(s)$ is the Dirac function. The coefficients H, P, M, and T are defined as follows:

$$H = \frac{\rho A d}{2m}\left(C_{L_\alpha} - C_D - \frac{md^2}{I_y}C_{M_q}\right) \tag{2}$$

$$P = \frac{I_x}{I_y}\frac{pd}{V} \tag{3}$$

$$M = \frac{\rho A d^3}{2I_y}C_{M_\alpha} \tag{4}$$

$$T = \frac{\rho A d}{2m}\left(C_{L_\alpha} + \frac{md^2}{I_x}C_{M_{p\alpha}}\right) \tag{5}$$

Figure 1 shows that the complex incidence angle is the plane projection of the total angle of attack. As the projectile travels along the trajectory, the complex incidence traces out a series of loops in the pitch-yaw plane, which is normal to the velocity vector. In Fig. 1, $\bar{\alpha}$ is the total incidence angle.

Figure 2 depicts the notations of the complex incidence, either in terms of pitch and yaw or in terms of magnitude $\|\xi\|$ and phase angle ϕ.

B. Complex Incidence Motion

The solution to Eq. (1) is given by the sum of the slow and fast arms (denoted S and F, respectively) of the epicyclic motion as follows:

$$\xi = K_{F_0}e^{[\lambda_F s + i(\phi_F' s + \phi_{F_0})]} + K_{S_0}e^{[\lambda_S s + i(\phi_S' s + \phi_{S_0})]} \tag{6}$$

The solution is valid for $s > 0$. For $s < 0$, the complex incidence ξ equals zero. This motion of the two arms is depicted in Fig. 3. In Eq. (6), ϕ_F' and ϕ_S' are the fast and slow arm turning rates, whereas λ_F and λ_S are the fast and slow arm damping exponents. These are defined as follows:

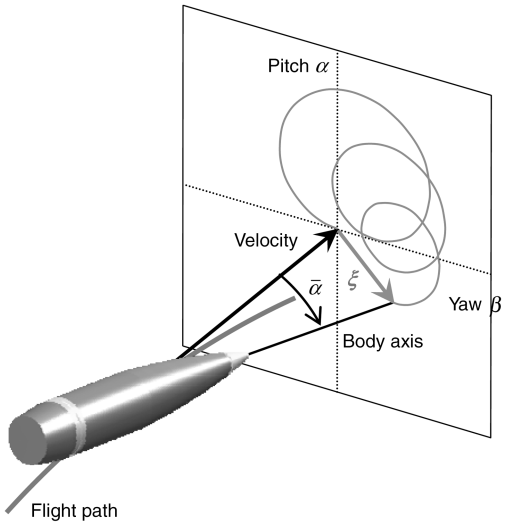

Fig. 1 Complex incidence in pitch-yaw plane.

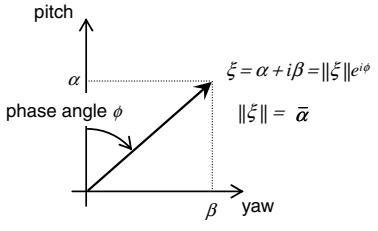

Fig. 2 Complex incidence.

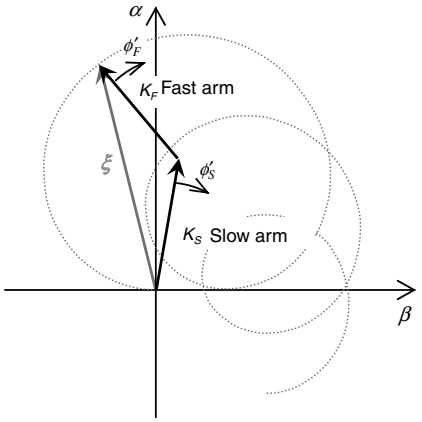

Fig. 3 Geometry of epicyclic pitching and yawing motions.

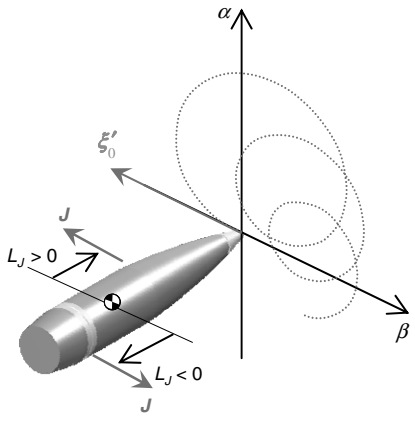

Fig. 4 Initiation of angular motion.

$$\phi'_F = \tfrac{1}{2}(P + \sqrt{P^2 - 4M}) \tag{7}$$

$$\phi'_S = \tfrac{1}{2}(P - \sqrt{P^2 - 4M}) \tag{8}$$

$$\lambda_F = -\frac{1}{2}\left(H - \frac{P(2T - H)}{\sqrt{P^2 - 4M}}\right) \tag{9}$$

$$\lambda_S = -\frac{1}{2}\left(H + \frac{P(2T - H)}{\sqrt{P^2 - 4M}}\right) \tag{10}$$

Neglecting the damping exponents, which are an order of magnitude smaller than the turning rates, the initial amplitudes and phase angles of the fast and slow arms are defined by the initial conditions of the yaw motion as follows:

$$K_{F_0} e^{i\phi_{F_0}} = -\frac{i\xi'_0 + \phi'_S \xi_0}{\phi'_F - \phi'_S} \tag{11}$$

$$K_{S_0} e^{i\phi_{S_0}} = \frac{i\xi'_0 + \phi'_F \xi_0}{\phi'_F - \phi'_S} \tag{12}$$

C. Initial Conditions

The initial conditions of the motion are determined by the lateral Dirac impulse J that is defined in the pitch-yaw frame by its amplitude and its phase angle as follows:

$$J = \|J\| e^{i\phi_J} \tag{13}$$

J is applied at L_J calibers from the center of mass. Note that the same motion can be triggered using two opposite locations of the impulse, as shown in Fig. 4.

In Eqs. (11) and (12), the initial incidence of the projectile following an impulse thruster detonation of magnitude J and orientation ϕ_J can be estimated from the ratio of the impulse momentum and the projectile momentum:

$$\xi_0 = \frac{1}{mV} J e^{i\phi_J} \tag{14}$$

The initial yaw rate can be obtained from a balance of the angular momentum:

$$\xi'_0 = \frac{L_J d^2}{I_y V} J e^{i\phi_J} \tag{15}$$

In supersonic mode, ξ_0 can be neglected. Thus, ξ'_0 is the main cause of the angular motion (unless $L_J \to 0$, but this case is not taken into consideration here).

D. Analytical Solution for Aerodynamically Induced Impulses

Using the analytically derived equation for the complex incidence [Eq. (6)], the complex deflection velocity $V_L e^{i\phi_{V_L}}$ or the lift impulse J_L due to the lift force L resulting from the yawing motion can be computed as

$$J_L = mV_L e^{i\phi_{V_L}} = \int_0^\infty L(t)\,\mathrm{d}t = \int_0^\infty L(s)\frac{d}{V}\,\mathrm{d}s = \int_0^\infty \left(\frac{1}{2}\rho A V^2 C_{L_\alpha}\xi\right)\frac{d}{V}\,\mathrm{d}s = \frac{1}{2}\rho A V d C_{L_\alpha}\int_0^\infty \xi\,\mathrm{d}s \tag{16}$$

The difference between ϕ_J and ϕ_{V_L} is the included angle between the axes defined by J and J_L. It can reach a few degrees for a standard artillery shell, whereas it is only a fraction of a degree for fin-stabilized shell. Thus, the vectors J and J_L are roughly aligned along the same axis, either in the same direction or in opposite directions. Similarly, the loss of velocity V_{D_2} due to the additional drag D_2 resulting from the yaw motion can be defined as

$$J_{D_2} = mV_{D_2} = \int_0^\infty D_2(t)\,\mathrm{d}t = \int_0^\infty D_2(s)\frac{d}{V}\,\mathrm{d}s = \int_0^\infty \left(\frac{1}{2}\rho A V^2 C_{D_2}|\xi|^2\right)\frac{d}{V}\,\mathrm{d}s = \frac{1}{2}\rho A V d C_{D_2}\int_0^\infty |\xi|^2\,\mathrm{d}s \tag{17}$$

assuming that $C_D = C_{D_0} + C_{D_2}|\xi|^2$. It should be noted that the complex incidence of squared ξ^2 is used only to calculate the additional drag arising from the angular motion of the projectile following the activation of an impulser.

The impulse resulting from the Magnus force may be significant for spin-stabilized shells. It is simply defined as a function of the lift impulse as follows:

$$J_Y = i\frac{C_{Yp\alpha}}{C_{L\alpha}}\frac{pd}{V}J_L \tag{18}$$

Using Eq. (6) and assuming that $\lambda_F < 0$ and $\lambda_S < 0$, the definite integrals of ξ and ξ^2 can be determined. The definite integral ξ and $|\xi|^2 = \xi\bar{\xi}$ in Eqs. (16) and (17) are given by

$$\int_0^\infty \xi\,\mathrm{d}s = -\frac{K_{F_0} e^{i\phi_{F_0}}}{\lambda_F + i\phi'_F} - \frac{K_{S_0} e^{i\phi_{S_0}}}{\lambda_S + i\phi'_S} \tag{19}$$

$$\int_0^\infty |\xi|^2\,\mathrm{d}s = -\frac{K_{F_0}^2}{2\lambda_F} - \frac{K_{S_0}^2}{2\lambda_S} - \frac{2K_{F_0}K_{S_0}[(\lambda_F + \lambda_S)\cos(\phi_{F_0} - \phi_{S_0}) + (\phi'_F - \phi'_S)\sin(\phi_{F_0} - \phi_{S_0})]}{(\lambda_F + \lambda_S)^2 + (\phi'_F - \phi'_S)^2} \tag{20}$$

Equations (16–20) constitute the full analytical solution of the aerodynamic impulses caused by the angular motion. They are valid for both spin- and fin-stabilized projectiles. In Eqs. (11) and (12), the

initial yaw ξ_0 could have been set to zero in order to simplify the integration process in Eqs. (19) and (20). However, in order to maintain generality, it was left in the equations.

E. Simplified Solution for Lift Impulse

Substituting Eq. (19) in Eq. (16), the lift impulse or aerodynamic jump can be rewritten as

$$J_L = -\frac{1}{2}\rho AVdC_{L_\alpha}\left[\frac{K_{F_0}e^{i\phi_{F_0}}}{\lambda_F + i\phi'_F} + \frac{K_{S_0}e^{i\phi_{S_0}}}{\lambda_S + i\phi'_S}\right] \tag{21}$$

or

$$J_L = -\frac{1}{2}\rho AVdC_{L_\alpha}\left[\left(\frac{\lambda_F - i\phi'_F}{\lambda_F^2 + \phi_F'^2}\right)K_{F_0}e^{i\phi_{F_0}} + \left(\frac{\lambda_S - i\phi'_S}{\lambda_S^2 + \phi_S'^2}\right)K_{S_0}e^{i\phi_{S_0}}\right] \tag{22}$$

As mentioned by McCoy [15], the damping exponents are, in general, between one and two orders of magnitude smaller than the epicyclic turning rates. Thus, a very decent approximation to Eq. (21) can be written as follows:

$$J_L = i\frac{1}{2}\rho AVdC_{L_\alpha}\left[\frac{K_{F_0}}{\phi'_F}e^{i\phi_{F_0}} + \frac{K_{S_0}}{\phi'_S}e^{i\phi_{S_0}}\right] \tag{23}$$

Substituting Eqs. (11) and (12) into Eq. (23), one obtains

$$J_L = i\frac{1}{2}\rho AVdC_{L_\alpha}\left[\frac{-i\xi'_0 - \phi'_S\xi_0}{\phi'_F(\phi'_F - \phi'_S)} + \frac{i\xi'_0 + \phi'_F\xi_0}{\phi'_S(\phi'_F - \phi'_S)}\right] \tag{24}$$

Now, $M = \phi'_F\phi'_S - \lambda_F$, $\lambda_S = (\rho Ad^3/2I_y)C_{M\alpha} \approx \phi'_F\phi'_S$, and $P = \phi'_F + \phi'_S$. Substituting these in Eq. (24), the following simplified expression for the lift impulse is obtained:

$$J_L = i\frac{1}{2}\rho AVdC_{L_\alpha}\left[\frac{-i\xi'_0 + P\xi_0}{M}\right] \tag{25}$$

or

$$J_L = V\frac{I_y}{d^2}\frac{C_{L_\alpha}}{C_{M_\alpha}}[iP\xi_0 - \xi'_0] \tag{26}$$

In Eq. (26), the initial yaw ξ_0 is usually very small, since the thruster impulse is much smaller than the projectile total momentum in Eq. (14). It can therefore be neglected in Eq. (26). Assuming that ξ'_0 is the major cause of the forced epicyclic motion, the relation between the lift impulse J_L and the thruster impulse J can be derived by substituting Eq. (15) into Eq. (26). This yields the following relationship between J and J_L:

$$J_L = -JL_J\frac{C_{L\alpha}}{C_{M\alpha}}e^{i\Delta\phi_J} \tag{27}$$

where $\Delta\phi_J$ is the included angle between the axes defined by J and J_L. If ξ'_0 is the major cause of the forced epicyclic motion, $\Delta\phi_J$ is a few degrees for a standard artillery shell and a fraction of a degree for fin-stabilized projectiles. Thus, neglecting the phase shift $\Delta\phi$, J_L and J have the same direction for fin-stabilized projectiles ($C_{M\alpha} < 0$), whereas J_L and J have opposite directions for spin-stabilized projectiles ($C_{M\alpha} > 0$). This basic result is illustrated in Figs. 5 and 6. Figure 5 depicts the angular motion of a slowly rolling fin-stabilized shell (spin = 20 Hz) assuming an upward initial condition. The resulting lift impulse is also oriented upward. Figure 6 depicts the angular motion of a spin-stabilized shell (spin = 200 Hz) assuming an upward initial condition. The resulting lift impulse is oriented downward due to the gyroscopic effect. The side (Magnus) impulse J_Y is shifted by 90° to the left of J_L.

F. Angular Motion Equation for Paired Impulses

The angular motion induced by a pair of impulses can be modeled analytically as well. Considering two Dirac impulses J_1 and J_2 engaged at travel distances s_1 and s_2, both impulse vectors are normal

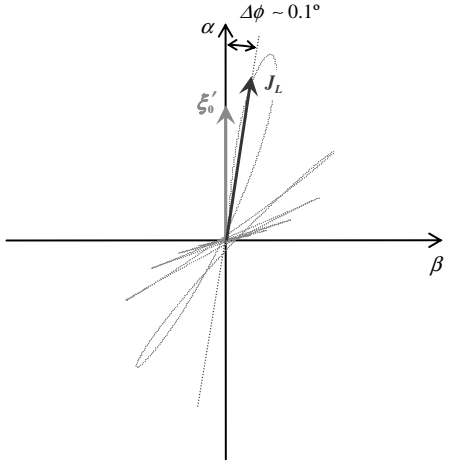

Fig. 5 Angular motion of a fin-stabilized projectile.

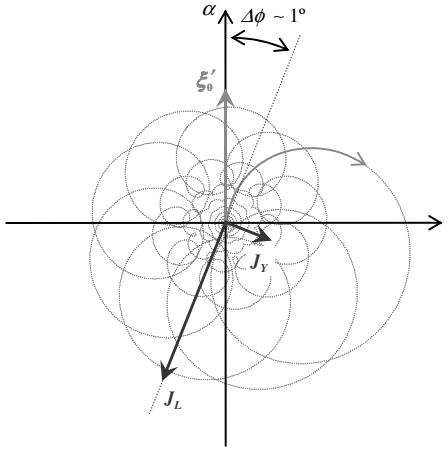

Fig. 6 Angular motion of a spin-stabilized projectile.

to the projectile axis and are applied at L_{J1} and L_{J2} calibers from the center of mass. Within the frame of the linearized equation of angular motion, the resulting complex angle is simply defined as $\xi = \xi_1 + \xi_2$, where ξ_1 and ξ_2 are phase-shifted epicyclic motions having the same frequencies but different initial conditions. The variables ξ_1 and ξ_2 are generated by the first and second impulse, respectively. As before, neglecting the steady-state yaw due to the gravity and introducing the effect of the impulse, the epicyclic pitching and yawing motions of a projectile can be represented by the following differential equation:

$$\xi'' + (H - iP)\xi' - (M + iPT)\xi = \xi'_{01}\delta(s - s_1) + \xi'_{02}\delta(s - s_2) \tag{28}$$

where ξ'_{01} and ξ'_{02} are the initial yaw rates generated by the first and second impulse, respectively. The solution to Eq. (28), the complex incidence, can be broken down into three parts as follows:

$$\xi(s < s_1) = \xi_1 + \xi_2 = 0 \tag{29}$$

$$\xi(s_1 < s < s_2) = \xi_1 = \xi'_{01}\frac{e^{(\lambda_f + i\phi'_f)(s_1 - s)} - e^{(\lambda_s + i\phi'_s)(s_1 - s)}}{i(\phi'_f - \phi'_s)} \tag{30}$$

$$\xi(s_1 < s < s_2) = \xi_1 + \xi_2 = \xi'_{01}\frac{e^{(\lambda_f + i\phi'_f)(s_1 - s)} - e^{(\lambda_s + i\phi'_s)(s_1 - s)}}{i(\phi'_f - \phi'_s)} + \xi'_{02}\frac{e^{(\lambda_f + i\phi'_f)(s_2 - s)} - e^{(\lambda_s + i\phi'_s)(s_2 - s)}}{i(\phi'_f - \phi'_s)} \tag{31}$$

III. Optimization Technique Using Paired Impulses

To optimize the use of impulse on spin- and fin-stabilized projectiles, a projectile of mass m traveling at velocity V is considered. A Dirac impulse J is engaged at some travel distance s. The impulse vector is normal to the projectile axis and is applied either aft or forward of the center of gravity. This event forces the oscillation of the projectile, which yields three impulses due to the aerodynamic forces, as shown in Fig. 7: two transverse impulses J_L and J_Y due to the action of the lift and Magnus forces and one axial impulse J_{D2} due to the squared-yaw component of the drag force. Assuming a constant velocity V, the total angular deflection of the trajectory is then simply given by

$$a = \frac{\|J + J_L + J_Y\|}{mV} \tag{32}$$

In the following subsections, rules will be established to properly pair impulse thrusters in order to achieve a maximum trajectory correction while minimizing the range lost due to the drag induced by the angular motion.

A. Rule 1: Impulse Axial Location Relative to Center of Mass

To maximize the angular deflection, the sum of the impulse $J + J_L$ must be maximized in Eq. (32). This can be achieved if the thruster impulse J and the resulting lift impulse J_L are aligned in the same direction. For a spin-stabilized shell, this condition is met if the impulse thrusters are fired behind the center of mass, as shown in Fig. 8. This can be demonstrated physically by looking at Fig. 9. In this figure, a thruster is triggered on the port side of the projectile, resulting in a rightward-pointing impulse J. This impulse initiates the angular motion of the projectile. The resulting initial yaw rate ξ_0' and the initial angular motion of the projectile are to the left. However, the gyroscopic response rapidly pitches up the nose of the projectile and,

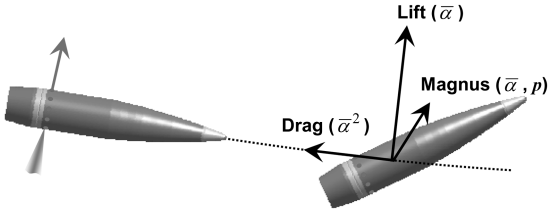

Fig. 7 Forces due to total incidence $\bar{\alpha}$.

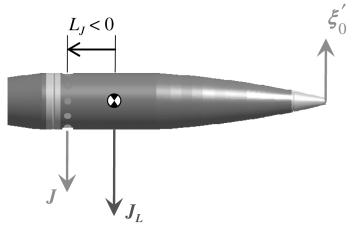

Fig. 8 Spin-stabilized projectile: J applied behind center of mass.

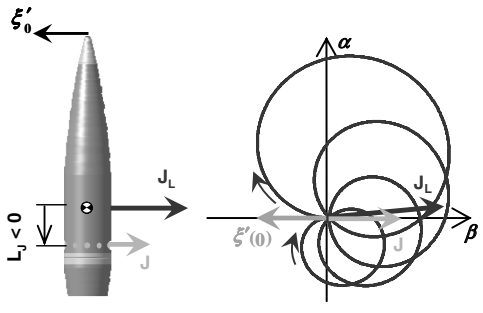

Fig. 9 Effect of an impulse on projectile angular motion.

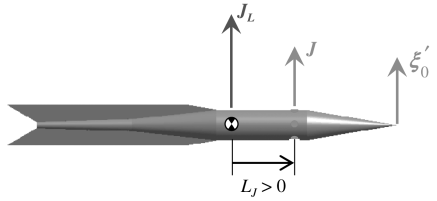

Fig. 10 Fin-stabilized projectile: J applied ahead of center of mass.

eventually, the resulting yaw motion is primarily oriented to the right of the projectile. Therefore, the net lift impulse J_L is oriented in the same direction as the thruster impulse to the right, as shown in Fig. 9. For a fin-stabilized projectile, there is no gyroscopic response. Therefore, the thrusters must be located forward of the center of mass for the lift impulse to be in the same direction as the thruster impulse, as illustrated in Fig. 10.

Rule 1 can now be defined in order to maximize $J + J_L$ (i.e., J must have the same direction than J_L): J must be applied ahead of the center of mass for fin-stabilized projectiles ($L_J > 0$ and $C_{M\alpha} < 0$), whereas J must be applied behind the center of mass for spin-stabilized projectiles ($L_J < 0$ and $C_{M\alpha} > 0$).

B. Rule 2: Angular Orientation of Second Impulse Relative to First One

To maximize the trajectory deflection and minimize the additional drag due to the forced oscillation, impulses can be paired. Consider two Dirac impulses J_1 and J_2 that are engaged at travel distances s_1 and s_2. Both impulse vectors are normal to the projectile axis and are applied at L_{J1} and L_{J2} calibers from the center of mass. Within the frame of the linearized equation of the angular motion, the resulting complex angle is simply defined as $\xi = \xi_1 + \xi_2$, where ξ_1 and ξ_2 are phase-shifted epicyclic motions having the same frequencies but different initial conditions, as shown in Fig. 11. Under the assumption of linearity, the total deflection angle is

$$a = \frac{\|J_1 + J_{1L} + J_{1Y} + J_2 + J_{2L} + J_{2Y}\|}{mV} \tag{33}$$

where transverse impulse J_L imparted by the lift force is then given by

$$J_L = \frac{1}{2}\rho AVdC_{L_\alpha}\left(\int_{s_1}^{\infty} \xi_1 \, \mathrm{d}s + \int_{s_2}^{\infty} \xi_2 \, \mathrm{d}s\right) = J_{1L} + J_{2L} \tag{34}$$

The angle α is independent of s_1 and s_2, since the transverse impulse in Eq. (34) is also independent of the impulse triggering location. It only depends on the orientation of each vector. This leads to rule 2, which can be stated as follows: the transverse impulse is a maximum if J_1 and J_2 have the same direction (same roll orientation), assuming that the distances L_{J1} and L_{J2} both satisfy rule 1.

C. Rule 3: Timing Between Two Impulses

The second impulse should ideally stop the angular motion triggered by the first one and therefore limit the range lost due to the drag impulse. The additional drag impulse is defined by

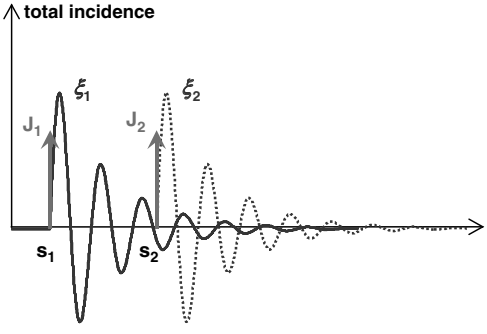

Fig. 11 Phase-shifted epicyclic motions.

$$J_{D_2} = \frac{1}{2}\rho AVdC_{D_2}\left(\int_{s_1}^{s_2} \xi_1^2\,\mathrm{d}s + \int_{s_2}^{\infty} (\xi_1 + \xi_2)^2\,\mathrm{d}s\right) \tag{35}$$

Note that if J_2 is applied when ξ_1 has already returned to zero (i.e., $s_2 \gg s_1$), then ξ_1 and ξ_2 do not interact and the resulting drag impulse resumes to

$$J_{D_2-0} = \frac{1}{2}\rho AVdC_{D_2}\left(\int_{s_1}^{\infty} \xi_1^2\,\mathrm{d}s + \int_{s_2}^{\infty} \xi_2^2\,\mathrm{d}s\right) \tag{36}$$

Minimizing J_{D_2} consists of finding out the amplitude of J_2 and the minimal value of s_2 so that the definite integral from s_2 to ∞ in Eq. (35) is zero: the second impulse should ideally stop the motion triggered by the first one. Thus, ξ_1 and ξ_2 should have the same amplitudes and be in opposite phase. For simplicity, we will examine here the ideal motions for which ξ_0 can be neglected and have equal damping factors (i.e., $\lambda_F = \lambda_S$). In this case, the epicyclic motions periodically pass through zero, because the fast and slow arms always have the same length. The motions are strictly opposed if the following conditions are met:

$$\xi_1(s_2 - s_1) = \xi_2(0) = 0 \tag{37}$$

$$\xi_1'(s_2 - s_1) = -\xi_2'(0) \tag{38}$$

where the origin of each angular motion has been shifted to the respective impulse location along the flight path. Equation (37) yields the first constraint:

$$s_2 - s_1 = \frac{2k\pi}{\phi_F' - \phi_S'} \tag{39}$$

where k is an integer greater than zero. Thus, the traveled distance between the two impulses is a multiple of the cycle of the total yaw. Using Eq. (6) to determine the closed-form derivative of ξ for the ideal case, Eq. (38) determines J_2 and adds two constraints on s_2:

$$J_2 L_{J2} = J_1 L_{J1} e^{\lambda_F (s_2 - s_1)} \tag{40}$$

$$s_2 - s_1 = \frac{(2k_S + 1)\pi}{\phi_S'} = \frac{(2k_F + 1)\pi}{\phi_F'} \tag{41}$$

where k_S and k_F are integers. Equation (40) takes into account the damping factor of the motion, which might actually be ignored when dealing with the actual impulse thrusters. Note that Eq. (40) is consistent with rule 2, since it implies that J_1 and J_2 are aligned.

Minimizing s_2 in Eq. (41) requires distinguishing between fin- and spin-stabilized projectiles. With regard to fin-stabilized projectiles, we have $\phi_S' = -\phi_F' < 0$. This case simply yields $k_S = -1$, $k_F = 0$, and $k = 1$, which minimizes s_2. As far as spin-stabilized projectiles are concerned, we have $\phi_F' > \phi_S' > 0$. In this case, making $k_S = 0$ to minimize s_2, Eq. (41) requires that $\phi_F' = (2k_F + 1)\phi_S'$. Assuming that this ideal condition is satisfied (which is not true for real shells), Eq. (39) is obviously satisfied if

$$k = k_F = \frac{1}{2}\left(\frac{\phi_F'}{\phi_S'} - 1\right) \tag{42}$$

Figure 12 shows the effect of paired impulses in the case of an ideal motion. This example illustrates the case of a generic spin-stabilized projectile for which $k = 4$.

The ideal result described by Eq. (42) can be extended to real projectiles. The optimal distance $(s_2 - s_1)$ traveled along the trajectory between the two impulses is defined by rule 3:

$$s_2 - s_1 = k\frac{2\pi}{\phi_F' - \phi_S'} \tag{43}$$

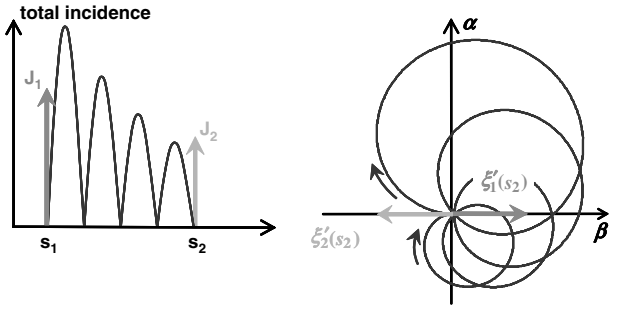

Fig. 12 Pairing of two impulses to stop projectile angular motion.

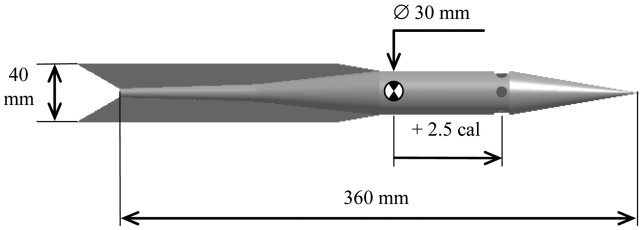

Fig. 13 Sketch of GSP shell.

$$k = \text{nearest integer to } \frac{\mathrm{sign}(\phi_S')}{2}\left(\frac{\phi_F'}{\phi_S'} - 1\right) \tag{44}$$

Equation (44) is valid for both fin- and spin-stabilized shells: $k = 1$ for fin-stabilized projectiles (regardless of spin), and $k > 1$ for spin-stabilized projectiles (depending on spin).

Equation (44) accounts for two conditions: the main condition is to trigger the second impulse at a minimum angle of attack, as defined by Eq. (37), and the subordinate condition is to shift the second impulse so that the angular motion is stopped or reduced to a large extent, as defined by Eq. (38).

IV. Results and Discussion

The results of the trajectory deflection caused by a pair of lateral impulses are examined in this section for both a spin- and a fin-stabilized projectiles: a standard 105-mm artillery shell and the French–German Research Institute of Saint-Louis (ISL) air-defense 30-mm fin-stabilized GSP shell. Comparisons between the analytical model predictions and 6-DOF simulations are made.

A. Guided Supersonic Projectile 30-Millimeter Fin-Stabilized Projectile

The ISL GSP is a 30-mm fin-stabilized projectile designed to increase the effectiveness of air-defense guns against maneuvering targets. The ISL GSP shell is described in [1–3]. Figure 13 displays a sketch of the shell. The inertial and aerodynamic features of the projectile are summarized in Table 1.

The parameters defining a pair of impulses are listed in Table 2, and the deflection resulting from those are presented in Table 3. Table 4 summarizes the performance or scores of the paired impulse control.

The angular motion resulting from the pair of impulses is described by Figs. 14 and 15. These figures show that the angular motion is almost stopped by the second impulse. The latter is reduced by 35% with respect to the first impulse, taking into account the high damping factor of the angular motion.

The differences between the analytical results described in Table 3 and the corresponding 6-DOF results are negligible. As far as the maximum angle of attack (Fig. 14) and the total deviation velocity (Fig. 16) are concerned, the discrepancy is less than 1%. The variation of the aerodynamic coefficients due to the change in the

Table 1 Parameters of GSP shell (Mach 3.0)

Parameter	Value
d	0.030 m
m	0.707 kg
I_x	$8.71e-5\ \text{kg}\cdot\text{m}^2$
I_y	$5.04e-3\ \text{kg}\cdot\text{m}^2$
p	105 rad/s
C_{D0}	0.21
C_{D2}	13.10
$C_{L\alpha}$	7.64
$C_{M\alpha}$	−4.08
C_{Mq}	−300
$C_{Np\alpha}$	0
$C_{Mp\alpha}$	0

Table 2 Parameters of impulse control

Parameter	Value	Definition
J_1	2.0 N · s	J_1 is directed upward along pitch axis
L_J	+2.5 cal	Located ahead of center of mass
k	1	As defined by Eq. (44)
$s_2 - s_1$	1021 cal	As defined by Eq. (39)
J_2	1.3 N · s	As defined by Eq. (40) with $L_{J_2} = L_{J_1} = L_J$
$t_2 - t_1$	30.0 ms	Time shift between two impulses

Table 3 Deflection results

Parameter	Value	Definition
$\bar{\alpha}_{\max}$	13.3°	Maximum angle of attack
V_J	4.67 m/s	Lateral velocity imparted by control impulses $J_1 + J_2$ (i.e., without lift)
V_L	21.46 m/s	Lateral velocity imparted by lift force
$\Delta\phi$	0.1°	Phase shift between V_J and V_L
V_Y	0 m/s	Lateral velocity imparted by side force
a	25.6 mrad	Total deflection, as defined by Eq. (33)
V_{D2}	6.70 m/s	Minimized loss of velocity due to J_{D2}, as defined by Eq. (35)
V_{D2-0}	19.32 m/s	Loss of velocity due to J_{D2-0}, as defined by Eq. (36)

Table 4 Scores of control

Parameter	Value	Definition
L score	4.59	Lift score (gain) $= V_L/V_J$ The higher, the better
D score	0.35	Drag score (reduction) $= V_{D2}/V_{D2-0}$ The lower, the better

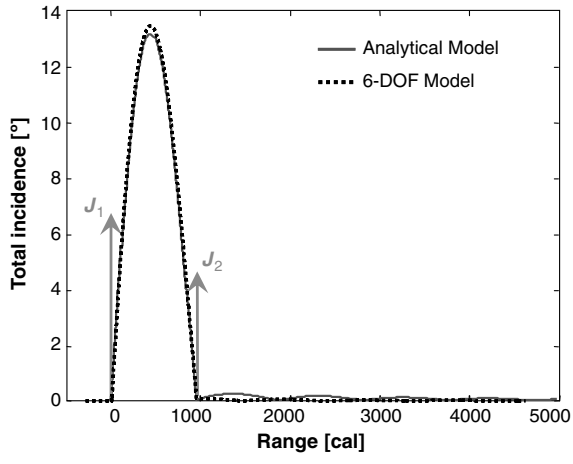

Fig. 14 Total angle of attack (GSP shell).

projectile velocity can be obviously neglected over the time interval between the two impulses.

B. 105-Millimeter Spin-Stabilized Artillery Projectile

The baseline spin-stabilized projectile configuration used for this project is shown in Fig. 17. It consists of a 105-mm M1 artillery projectile. The nominal projectile weight is 15.0 kg, and its length is 494 mm. The muzzle velocity of the projectile was taken to be 506 m/s, which is essentially that obtained when launched from the LG1 MK2 Howitzer. The spin rate of the projectile was set at 1682 rad/s. The inertial and aerodynamic features of the projectile are summarized in Table 5.

The parameters defining a pair of impulses are listed in Table 6, and the deflection resulting from those are presented in Table 7. Table 8 summarizes the performance or scores of the paired impulse control.

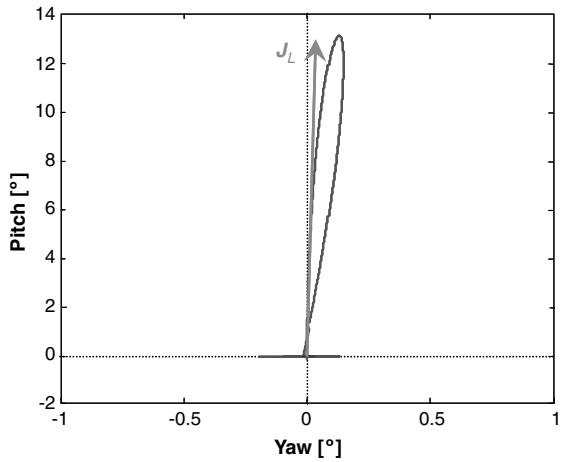

Fig. 15 Pitch versus yaw (GSP shell).

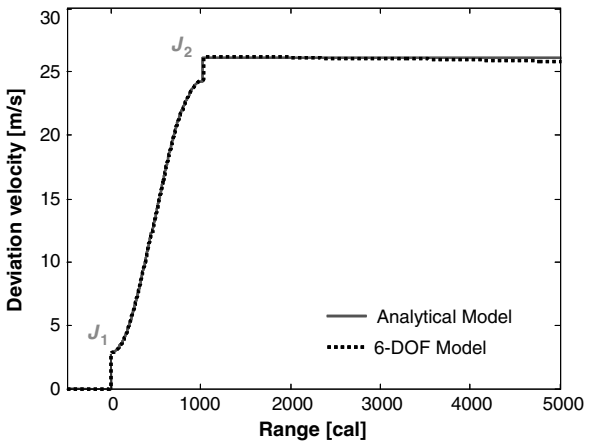

Fig. 16 Deviation velocity (GSP shell).

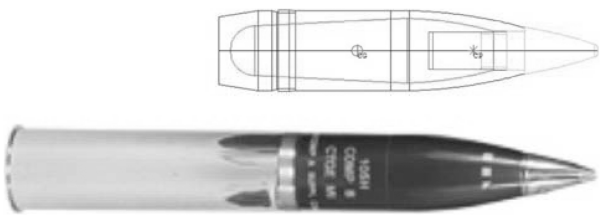

Fig. 17 105-mm M1 artillery projectile together with the projectile rocket ordinance design and analysis system (PRODAS) model used for simulation.

Table 5 Parameters of 105-mm artillery shell (Mach 1.5)

Parameter	Value
d	0.105 m
m	15.05 kg
I_x	$2.369e-2$ kg · m^2
I_y	$2.190e-1$ kg · m^2
p	1950 rad/s
C_{D0}	0.375
C_{D2}	7.7
$C_{L\alpha}$	2.12
$C_{M\alpha}$	3.6
C_{Mq}	−8.5
$C_{Np\alpha}$	−0.40
$C_{Mp\alpha}$	0.20

Table 6 Parameters of impulse control

Parameter	Value	Definition
J_1	10.0 N · s	J_1 is directed rightward along yaw axis
L_J	−0.5 cal	Located aft of center of mass
k	8	As defined by Eq. (44)
$s_2 - s_1$	1293 cal	As defined by Eq. (39)
J_2	8.0 N · s	As defined by Eq. (40) with $L_{J_2} = L_{J_1} = L_J$
$t_2 - t_1$	270 ms	Time shift between two impulses

Table 7 Deflection results

Parameter	Value	Definition
$\bar{\alpha}_{\max}$	1.5°	Maximum angle of attack
V_J	1.2 m/s	Lateral velocity imparted by control impulses $J_1 + J_2$ (i.e., without lift)
V_L	0.4 m/s	Lateral velocity imparted by lift force
$\Delta\phi$	9.5°	Phase shift between V_J and V_L
V_Y	0.027 m/s	Lateral velocity imparted by side force
a	3.0 mrad	Total deflection, as defined by Eq. (33)
V_{D2}	0.05 m/s	Minimized loss of velocity due to J_{D2}, as defined by Eq. (35)
V_{D2-0}	0.16 m/s	Loss of velocity due to J_{D2-0}, as defined by Eq. (36)

Table 8 Scores of control

Parameter	Value	Definition
L score	0.33	Lift score (gain) $= V_L/V_J$ The higher, the better
D score	0.31	Drag score (reduction) $= V_{D2}/V_{D2-0}$ The lower, the better

The angular motion resulting from the pair of impulses is described by Figs. 18 and 19. These figures show that the angular motion is almost stopped by the second impulse. The latter is reduced by 20% with respect to the first impulse, taking into account the high damping factor of the angular motion.

To show the viability of the analytical method at predicting the motion of a spin-stabilized projectile subjected to a pair of impulses, analytical and 6-DOF computations were performed for the generic 105-mm M1 artillery projectile.

Comparisons of the incidence variation with range for both the analytical method and the 6-DOF simulation show that there is a slight discrepancy of about 0.1° (Fig. 20). However, it can be shown that this difference essentially corresponds to the yaw of repose, which is not taken into account in the analytical solution. Furthermore, a complete aerodynamic model was used for the 6-DOF simulation, whereas only constant coefficients were used for the analytical computations. Other than that, the analytical model predicts the angular motion of the projectile very well.

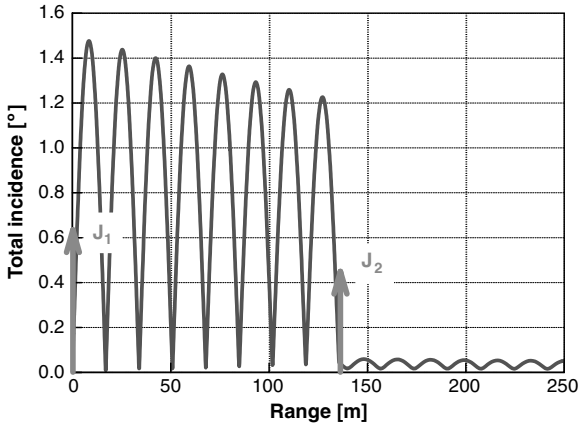

Fig. 18 Incidence variation with range following detonation of 10 Ns impulse thruster J_1 and 7.83 Ns impulse thruster J_2.

In Fig. 21, the variation of the lateral velocity imparted by the thruster as a function of range is shown for the 6-DOF simulation and the analytical calculations. For reasons mentioned previously, small discrepancies can be observed. However, the final lateral velocity immediately following the second velocity is predicted quite well.

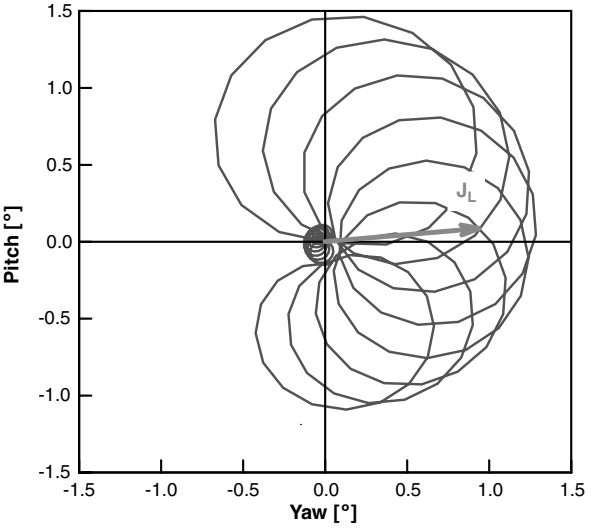

Fig. 19 Pitch versus yaw variation following detonation of 10 Ns impulse thruster J_1 and 7.83 Ns impulse thruster J_2.

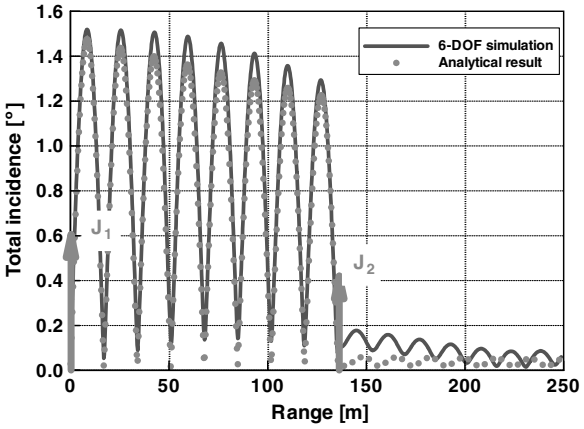

Fig. 20 Incidence variation with range following detonation of 10 Ns impulse thruster $J1$ and 7.83 Ns impulse thruster $J2$.

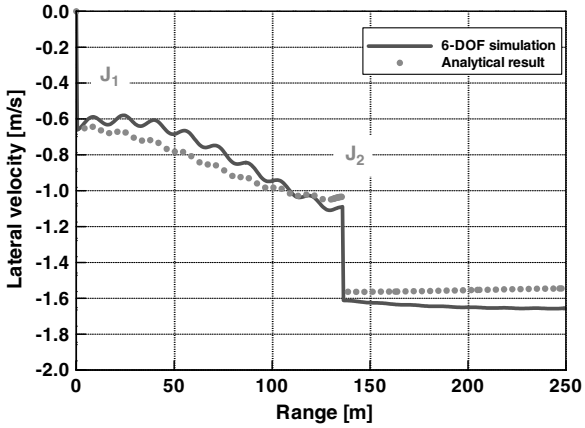

Fig. 21 Incidence variation with range following detonation of 10 Ns impulse thruster $J1$ and 7.83 Ns impulse thruster $J2$.

V. Conclusions

A novel method for correcting the trajectory of fin- or spin-stabilized projectiles using pairs of impulse thrusters was described in this report. By locating the impulse thrusters off the center of mass, it is possible to significantly increase the deflection of the flight path. This is explained by the fact that the deflection results from the aerodynamic jump due to the projectile oscillation in addition to the control impulses. To benefit from the added drift correction obtained by locating the thrusters off the center of mass and to avoid the added drag generated by the induced pitching and yawing motions, an optimal combination of the thrusters can be achieved by considering a pair of impulses, which has the double objective of maximizing the deflection and minimizing the drag due to the oscillation. Using the linearized equation of the angular motion and considering ideal cases, the optimization scheme was mathematically defined in the form of three simple rules. Using two test cases, it was shown that the correction technique is very effective for fin-stabilized projectiles, because the aerodynamic jump is maximized. On the contrary, the technique is not that effective regarding spin-stabilized projectiles. In this case, using thrusters located at the center of mass is less complex with only a small loss of effectiveness. The model developed as part of this project is expected to be useful to guided weapon control designers in providing simple rules and equations that can be applied to maximize course corrections of both fin- and spin-stabilized projectiles.

References

[1] Wey, P., Berner, C., Sommer, E., Fleck, V., and Moulard, H., "Theoretical Design for a Guided Supersonic Projectile," *Proceedings of the 22nd International Symposium on Ballistics*, Vancouver, edited by W. Flis, and B. Scott, Vol. 1, DEStech Publ., Lancaster, PA, 2005, pp. 120–127.

[2] Wey, P., "Performance Analysis of ISL's Guided Supersonic Projectile," *Proceedings of the 23rd International Symposium on Ballistics*, Tarragona, Spain, edited by F. Galvez, and V. Sanchez-Galvez, Vol. 1, Graficas Couche SL, Madrid, 2007, pp. 655–663.

[3] Berner, C., Sommer, E., Schirm, V., and Wey, P., "Preliminary Design for ISL's Guided Supersonic Projectile," *Proceedings of the 23rd International Symposium on Ballistics*, Tarragona, Spain, edited by F. Galvez, and V. Sanchez-Galvez, Vol. 1, Graficas Couche SL, Madrid, 2007, pp. 621–629.

[4] Wey, P., and Corriveau, D., "Trajectory Deflection of Fin- and Spin-Stabilized Projectiles Using Paired Lateral Impulses," *Proceedings of the 24th International Symposium on Ballistics*, New Orleans, LA, edited by S. Bless, and J. Walker, Vol. 1, DEStech Publ., Lancaster, PA, 2008, pp. 188–197.

[5] Champigny, P., and Lacau, R. G., "Missiles Aerodynamics: Lateral Jet Control for Tactical Missiles," NATO, AGARD-R-804, 1994.

[6] Brandeis, J., and Gill, J., "Experimental Investigation of Super- and Hypersonic Jet Interaction on Missile Configurations," *Journal of Spacecraft and Rockets*, Vol. 35, No. 3, 1998, pp. 296–302. doi:10.2514/2.3354

[7] Horwath, T. G., and Barnych, G., "Low Cost Course Correction (LCCC) Technology Applications," *National Defense Industrial Association (NDIA) International Armaments Technology Symposium*, Parsippany, NJ, 2004, http://www.dtic.mil/ndia/2004armaments/DayII/SessionI/09_BarnychApplication_of_LCCC_Tech.pdf [retrieved 2011].

[8] Magnotti, P. J., Terhune, J., and Barnych, G., "Low Cost Course Correction (LC3) For Mortars Information Briefing," *38th Annual Gun, Ammunition and Missiles Symposium and Exhibition*, Monterey, CA, 2003, http://www.dtic.mil/ndia/2003gun/mag.pdf [retrieved 2011].

[9] Cooper, G. R., "Projectile Aerodynamic Jump Due to Lateral Impulsives," U.S. Army Research Laboratory, ARL-TR-3087, Aberdeen Proving Ground, MD, 2003.

[10] Burchett, B., Peterson, A., and Costello, M., "Prediction of Swerving Motion of a Dual-Spin Projectile With Lateral Pulse Jets in Atmospheric Flight," *Mathematical and Computer Modelling*, Vol. 35, No. 7, 2002, pp. 821–834. doi:10.1016/S0895-7177(02)00053-5

[11] Guidos, B. J., and Cooper, G. R., "The Effect of a Simple Lateral Impulse on Kinetic Energy Projectiles in Flight," U.S. Army Research Laboratory, ARL-TR-2076, Aberdeen Proving Ground, MD, Dec. 1999.

[12] Ollerenshaw, D., and Costello, M., "On the Swerve Response of Projectiles to Control Input," U.S. Army Research Laboratory, ARL-CR-0604, Aberdeen Proving Ground, MD, April 2008.

[13] English, B. A., Gadiraju, P., Rinehart, C. S., Glezer, A., and Allen, M. G., "Gas Generator Actuator Arrays for Flight Control of Spinning Body Projectiles," *19th IEEE International Conference on Micro-ElectroMechanical Systems (MEMS 2006)*, Istanbul, Turkey, IEEE Publ., Piscataway, NJ, 2006, pp. 806–809. doi:10.1109/MEMSYS.2006.1627922

[14] McCoy, R. L., "Linearized Pitching and Yawing Motion of Rotationally Symmetric Projectiles," *Modern Exterior Ballistics: The Launch and Flight Dynamics of Symmetric Projectiles*, Schiffer Publ., Atglen, PA, 1998, pp. 221–239.

[15] McCoy, R. L., "Linearized Swerving Motion of Rotationally Symmetric Projectiles," *Modern Exterior Ballistics: The Launch and Flight Dynamics of Symmetric Projectiles*, Schiffer Publ., Atglen, PA, 1998, pp. 240–251.